RSC Advances

PAPER

Cite this: *RSC Adv.*, 2016, **6**, 98197

Thermoelectric properties of the spin-polarized half-metallic ferromagnetic CsTe and RbSe compounds

A. H. Reshak*[ab]

The thermoelectric properties of the spin-polarized half-metallic ferromagnetic CsTe and RbSe compounds are investigated based on the calculated spin-polarized electronic band structures. The calculated spin-polarized electronic band structures show that both compounds exhibit a half-metallic gap of about 0.06 (0.07) eV for CsTe (RbSe). The spin-down channel of both compounds exhibits a density of states at the Fermi level (E_F), $N(E_F)$, and hence a bare electronic specific heat coefficient (γ) which should lead to unusual thermoelectric properties that is attributed to the fact that only the spin-down channel contributes to the states at E_F. Thus, the bands that cross E_F are responsible for the thermoelectric properties and the ones which do not cross E_F will contribute negligibly to the thermoelectric properties. It has been reported that the transport properties are related to the electrons in the system, and these electrons are defined through the Fermi surface, which determines the electrical conductivity therefore, the Fermi surface of the spin-down channels for both compounds are calculated. It has been found that CsTe exhibits a power factor as a function of chemical potential larger than that obtained from RbSe which is attributed to the fact that CsTe possesses much higher electronic electrical conductivity than that of RbSe.

Received 12th September 2016
Accepted 10th October 2016

DOI: 10.1039/c6ra22758a

www.rsc.org/advances

1. Introduction

Thermoelectric materials have become promising candidates to solve the global energy problems and a great alternative solution for energy and environment problems.[1–4] Recent review articles cover the basic physics of half-metallic ferromagnets (HMF)[5] and aspects of applications.[6,7] Due to their exceptional electronic band structures at the Fermi level (E_F), HMF materials have attracted much interest because they exhibit metallic character in one spin channel and semiconducting character in the other spin channel, resulting in complete spin polarization of electrons at E_F.[8] Therefore, they have received exceptional and great attention for possible use as spin-electronics materials, magneto-resistive devices and thermoelectric devices.[5–7]

The performance of the thermoelectric materials is defined by their dimensionless figure of merit $ZT = S^2\sigma T/k_e + k_l$,[9] where S, σ and $k_e + k_l$ are the Seebeck coefficient, electrical conductivity, the electronic thermal conductivity and the lattice thermal conductivity. It has been found that the recent observation of the spin Seebeck effect allows to pass a pure spin current over a long distance[10] and is directly applicable to the production of spin voltage generators which are crucial for driving spintronics devices.[11–13] Therefore, we have performed comprehensive calculations for the spin-polarized half-metallic ferromagnetism RbSe and CsTe compounds using first-principles and second-principles methods to obtain the ground state thermoelectric properties.

2. Details of calculations

It has been reported that CsTe and RbSe compounds in CsCl structure have $Pm\bar{3}m$ (no. 221) space group with lattice constants $a = 4.621$ Å (CsTe) and $a = 4.167$ Å (RbSe).[14] In these structures Cs or Rb atom is situated at (0.0, 0.0, 0.0) whereas Te or Se atom occupied the site (0.5, 0.5, 0.5).[14] Previous results[14] show that the ferromagnetic CsCl structure is energetically the most stable for CsTe and RbSe compounds. Therefore, we have investigated the ground state properties and thermoelectric properties of CsTe and RbSe in CsCl structure. The crystal structure of CsTe and RbSe compounds is shown in Fig. 1a and b. The full potential linear augmented plane wave plus the local orbitals (FPLAPW + lo) method as implemented in WIEN2k code[15] within the generalized gradient approximation (PBE-GGA)[16] are used to optimize the lattice constant. The obtained lattice constant are $a = 4.623$ Å for CsTe and $a = 4.169$ Å for RbSe.

Using FPLAPW + lo within the recently modified Becke–Johnson potential (mBJ)[17] the electronic band structure of CsTe

[a]*New Technologies-Research Centre, University of West Bohemia, Univerzitni 8, 306 14 Pilsen, Czech Republic. E-mail: maalidph@yahoo.co.uk; Fax: +420 386 361255; Tel: +420 777729583*

[b]*School of Material Engineering, University Malaysia Perlis, 01007 Kangar, Perlis, Malaysia*

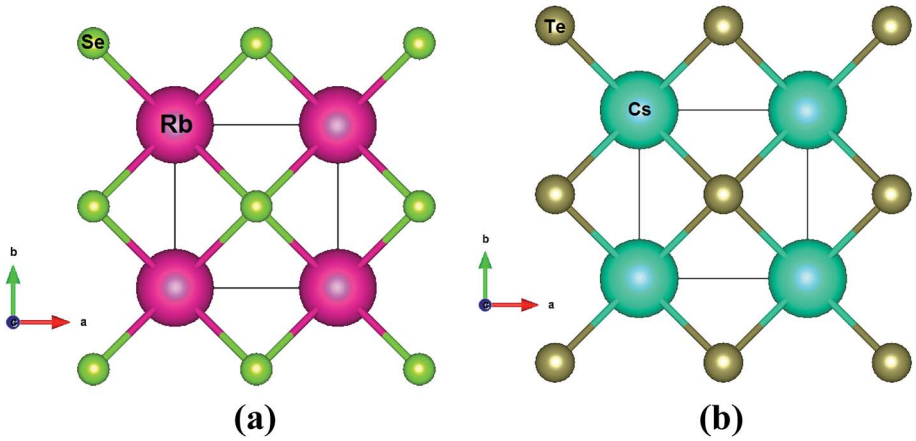

Fig. 1 The crystal structure of CsTe and RbSe compounds have $Pm\bar{3}m$ (no. 221) space group with lattice constants $a = 4.621$ Å (CsTe) and $a = 4.167$ Å (RbSe).[14] In these structures Cs or Rb atom is situated at (0.0, 0.0, 0.0) whereas Te or Se atom occupied the site (0.5, 0.5, 0.5).[14]

and RbSe compounds are calculated. Based on our previous results, the mBJ allows for the calculation of the band gaps with accuracy similar to the very expensive GW calculations. It is a local approximation to an atomic "exact-exchange" potential and a screening term.[17] From the obtained spin-polarized electronic band structures of the half-metallic CsTe and RbSe compounds, the spin-polarized thermoelectric properties are calculated utilizing the semi-classical Boltzmann theory as incorporated within BoltzTraP code, which solves the semi-classical Bloch-Boltzmann transport equations.[18] In general, the calculation of the thermoelectric properties is transition from first-principles to second-principles methods. The first-principles method used here is the FPLAPW + lo whereas the second-principles is the BoltzTraP code.[18] In general, the thermoelectric properties of the system are calculated from the ground state within the limits of Boltzmann theory[19–21] and the constant relaxation time approximation as implemented in the BoltzTraP code.[18] Usually BoltzTraP code performs a Fourier expansion of the quantum chemical band energies which allows to obtain the electronic group velocity v and inverse mass tensor, as the first and second derivatives of the bands with respect to k. Applying v and to the semiclassical Boltzmann equations, the transport tensors can be evaluated. In the current calculation the self-consistency is obtained using 900 $\vec{k}$ points in the irreducible Brillouin zone (IBZ). The self-consistent calculations are converged since the total energy of the system is stable within 0.00001 Ry. The spin-polarized electronic band structure and the thermoelectric properties of CsTe and RbSe compounds are calculated using 25 000 $\vec{k}$ points in the IBZ as the accurate calculations of thermoelectric properties of metals require the dense sampling of the BZ.

3. Results and discussion

The obtained spin-polarized electronic band structure of the half-metallic CsTe and RbSe compounds are shown in Fig. 2a, b, d and e. The spin-up channel exhibit a band gap of about 3.67 (3.94) eV for CsTe (RbSe) using mBJ approximation, in comparison with the previous calculated energy band gap 3.28 (3.40) eV for CsTe (RbSe) using full-potential local-orbital (FPLO) within PBE-GGA.[14] It is well-known that GGA usually underestimated the energy band gap therefore, we have used mBJ approach. Based on our previous results, the mBJ allows for the calculation of the band gaps with accuracy similar to the very expensive GW calculations. The spin-down channel exhibit metallic nature with three band cross E_F. Therefore, both compounds exhibit half-metallic magnets with half-metallic gap of about 0.06 (0.07) eV for CsTe (RbSe) therefore, these materials could act as an efficient thermoelectric materials. The spin-down channel of both compounds exhibit a density of states at E_F, $N(E_F)$, and hence a bare electronic specific heat coefficient (γ) (Table 1) which should lead to unusual transport properties that is attributed to the fact that only the spin-down channel contributes to the states at E_F. The same was previously observed by Kübler and Williams[22] in Co_2MnAl and Co_2MnSn compounds. Thus, the bands that cross E_F are responsible for the thermoelectric properties and the ones which are not crossing E_F will contribute negligibly small to the thermoelectric properties.[23] It has been reported that the thermoelectric properties is related to the electrons in the system, and these electrons are defined through Fermi surface, which determine the electrical conductivity.[22,23] Thus, as step forward we have calculated Fermi surface of the spin-down channel and the electronic charge density distribution for the spin-up/down channels to gain deep insight about the charge transfer and the chemical bonding nature.

The obtained Fermi surface for the spin-down channels of CsTe and RbSe compounds are shown in Fig. 2c and f–h. It has been noticed that the Fermi surface consist of white and colored sheets. The white sheets are corresponding to the holes concentration while the color ones are belong to the electrons concentration. Thus, following Fig. 2c and f–h the Fermi surface of CsTe and RbSe compounds is rich with electrons. Moreover, these colored sheets represent the speed of the electrons mobility; red the highest mobility and violet the lowest ones. Therefore, CsTe exhibit low electron's mobility at the center of

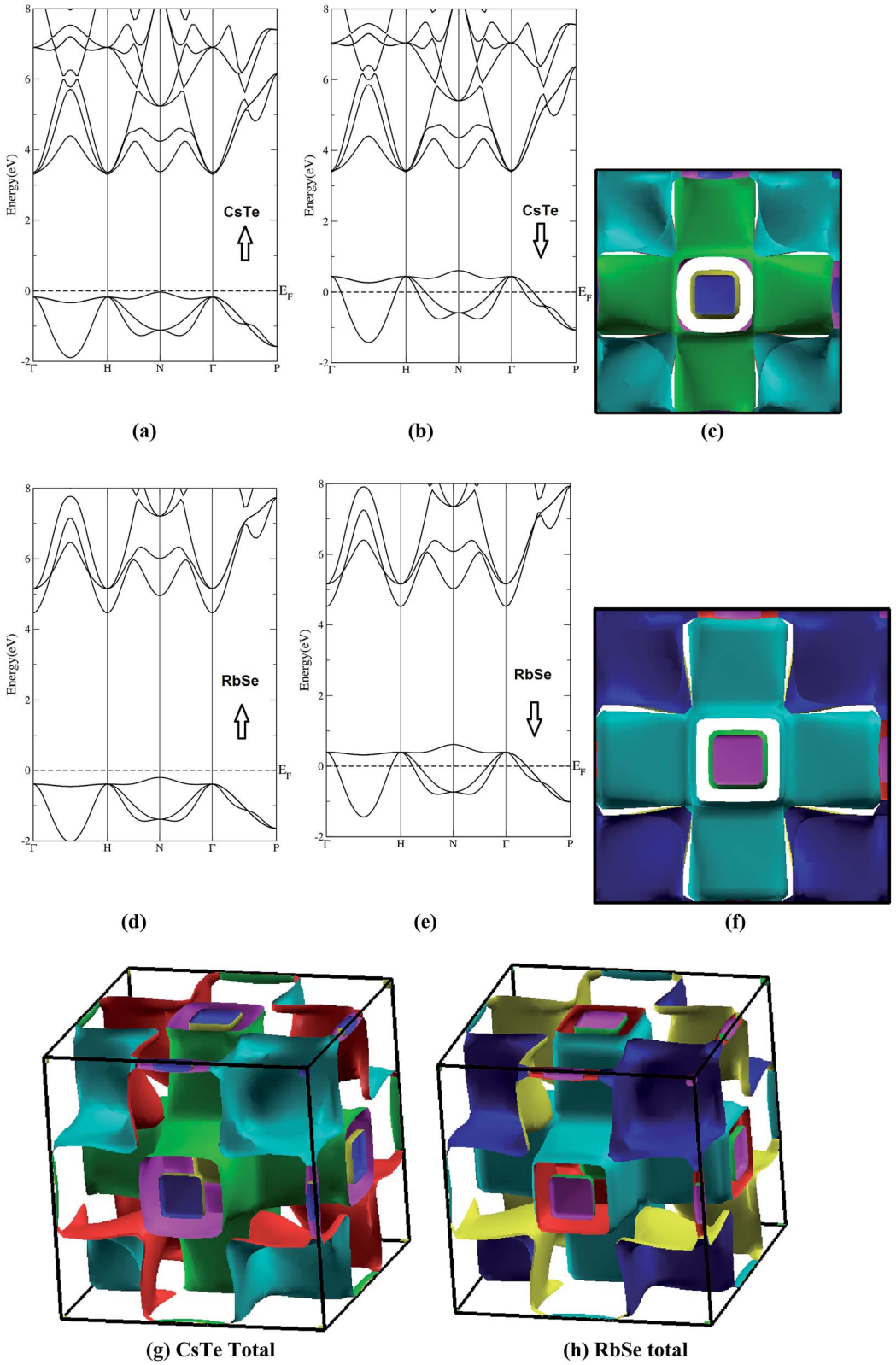

Fig. 2 (a and b) The spin-polarized electronic band structures of CsTe; (c) Fermi surface of spin-down channel of CsTe; (d and e) the spin-polarized electronic band structures of RbSe; (f) Fermi surface of spin-down channel of RbSe; (g and h) the 3D-image of Fermi surface of spin-down channel of CsTe and RbSe.

Table 1 Calculated density of states at E_F, $N(E_F)$, in (state per eV per unit cell) and the calculated bare electronic specific heat coefficient (γ) in mJ K^{-2} mol^{-1} per cell

CsTe			RbSe		
	$N(E_F)$	γ		$N(E_F)$	γ
Total DOS	19.99	3.46	Total DOS	19.72	3.42
Cs-Total	0.50	0.09	Rb-Total	0.35	0.06
Cs-6s	0.02	0.00	Rb-5s	0.02	0.00
Cs-5p	0.35	0.06	Rb-4p	0.19	0.03
Cs-4d	0.13	0.02	Rb-3d	0.13	0.02
Te-Total	9.19	1.59	Se-Total	12.38	2.15
Te-5s	0.04	0.01	Se-4s	0.04	0.01
Te-5p	9.13	1.58	Se-4p	12.32	2.14
Te-4d	0.02	0.00	Se-3d	0.02	0.00

the BZ whereas RbSe show the highest electron's mobility at the center of BZ. Further, we have investigated the valence electron charge density distribution for the spin-up/down channels of CsTe and RbSe compounds in two different crystallographic planes. The (1 0 0) crystallographic plane show one type of atoms Cs or Rb (Fig. 3a–d), which are surrounding by uniform spheres. While the (1 0 1) crystallographic plane (Fig. 3e–h) show both types of atoms.

The electro-negativity of Cs, Te, Rb and Se atoms are 0.79, 2.1, 0.81 and 2.55, respectively therefore, we found that the electro-negativity differences between Cs and Te atoms is 1.31 while between Rb and Se atoms is 1.74 which indicated the covalent bonding between Cs and Te also between Rb and Se. Following the (1 0 1) plane we can see that there is a charge transfer from Rb (Cs) atoms towards Se (Te) atoms, as it has been seen that the Se (Te) atoms are surrounded by uniform blue (green) spheres which indicate the maximum charge accumulation according to thermoscale (Fig. 3i).

We obtained the values of the spin magnetic moments for the atom resolved within the muffin-tin spheres and in the interstitial sites. These values in the unit of μ_B are listed in Table 2. The obtained spin magnetic moments are in accordance with the Slater–Pauling rule. Table 2 show that the magnetic moment of Se and Te atoms is the highest among the others. The calculated magnetic moment agree well with the previous theoretical results.[14] From the calculated spin-polarized electronic band structure we have obtained the thermoelectric properties for the spin-up/down channels and hence the total thermoelectric properties of CsTe and RbSe compounds using the BoltzTraP code.[18] Fig. 4a show the temperature dependent carrier concentration (n) for the spin-up channel of CsTe, it is clear that below 750 K the material possesses only n-type conductions whereas above 750 K the material turn to be p-type. The n-/p-types conductions increases with increasing the temperature. The spin-down channel of CsTe exhibit only the p-type conductions which reduces with increasing the temperature as shown in Fig. 4b. The temperature dependent carrier concentration for the spin-up/down channels of RbSe (Fig. 4c and d) show only n-type conductions. In general, there is a significant reduction in carrier concentration with increasing the temperature. The observed

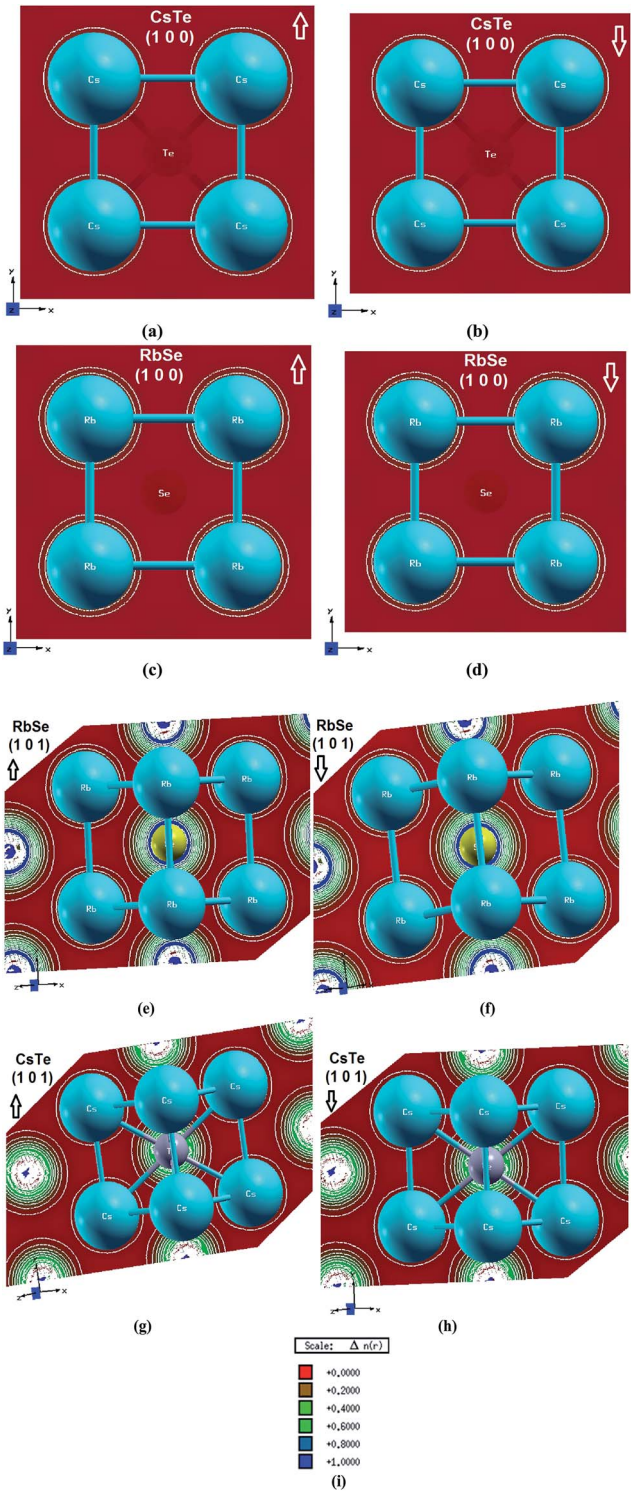

Fig. 3 (a–d) The crystallographic plane (1 0 0) of CsTe and RbSe; (e–h) the crystallographic plane (1 0 1) of CsTe and RbSe; (i) thermoscale.

trends in the carrier concentration for the spin-up/down confirm the half-metallic (HM) nature of CsTe and RbSe. Fig. 4e and f illustrated the total carrier concentration for CsTe and RbSe, it is clear that CsTe possesses only p-type conductions which increases exponentially with the T, while RbSe

Table 2 Calculated atom-resolved spin magnetic moment (in μ_B) along with the previous theoretical result[14]

CsTe			
M_{Cs} (μ_B)	M_{Te} (μ_B)	$M_{Interst.}$ (μ_B)	M_{tot} (μ_B)
0.01201	0.53387	0.45506	1.00094 1.00[a]
RbSe			
M_{Rb} (μ_B)	M_{Se} (μ_B)	$M_{Interst.}$ (μ_B)	M_{tot} (μ_B)
0.00655	0.72195	0.26483	0.99333 1.00[a]

[a] Ref. 14.

Table 3 Calculated the electron effective mass ratio (m_e^*/m_e), effective mass of the heavy holes (m_{hh}^*/m_e) and light holes (m_{lh}^*/m_e)

	CsTe		RbSe	
	Spin-up	Spin-down	Spin-up	Spin-down
m_e^*/m_e	0.00619	0.00545	0.00618	0.00583
m_{hh}^*/m_e	0.06691	0.05392	0.06866	0.05616
m_{lh}^*/m_e	0.02355	0.01877	0.02756	0.02204

possesses only n-type conductions which reduced with increasing T.

The electronic band structure of CsTe (RbSe) (Fig. 2a, b, d and e) show that the conduction band minimum (CBM) which is mainly formed by Cs-4d (Rb-3d) exhibit parabolic bands for spin-up/down channels, while the valence band minimum (VBM) which is mainly originated from Se-4p (Te-5p) show a flat

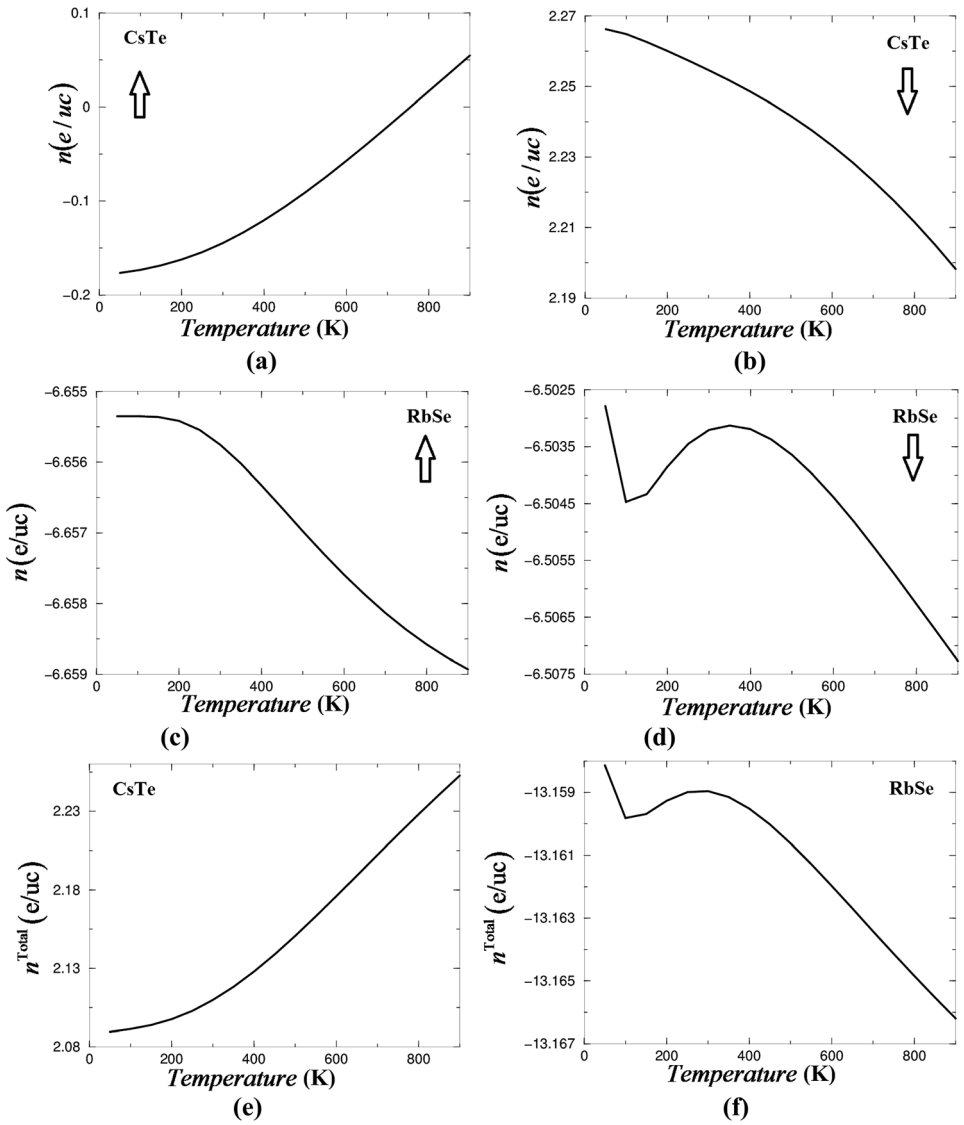

Fig. 4 (a and b) The temperature induced carrier concentration per unit cell (e per uc) of CsTe for (↑)(↓) electrons *versus* temperature; (c and d) the temperature induced carrier concentration per unit cell (e per uc) of RbSe for (↑)(↓) electrons *versus* temperature; (e and f) the total carrier concentration per unit cell (e per uc) of CsTe and RbSe *versus* temperature.

band for both spin-up/down channels. Whereas the valence band next to the VBM exhibit parabolic bands for spin-up/down channels. Which implies that the electrons in the CBM and the light holes in the second VB exhibit low effective mass (Table 3) and hence high mobility while in the VBM the heavy holes possesses high effective mass (Table 3) and hence low mobility. Therefore, CsTe and RbSe exhibit a maximum carrier concentration in the vicinity of E_F.

In general, good thermoelectric performance requires high electrical conductivity, large Seebeck coefficient and low

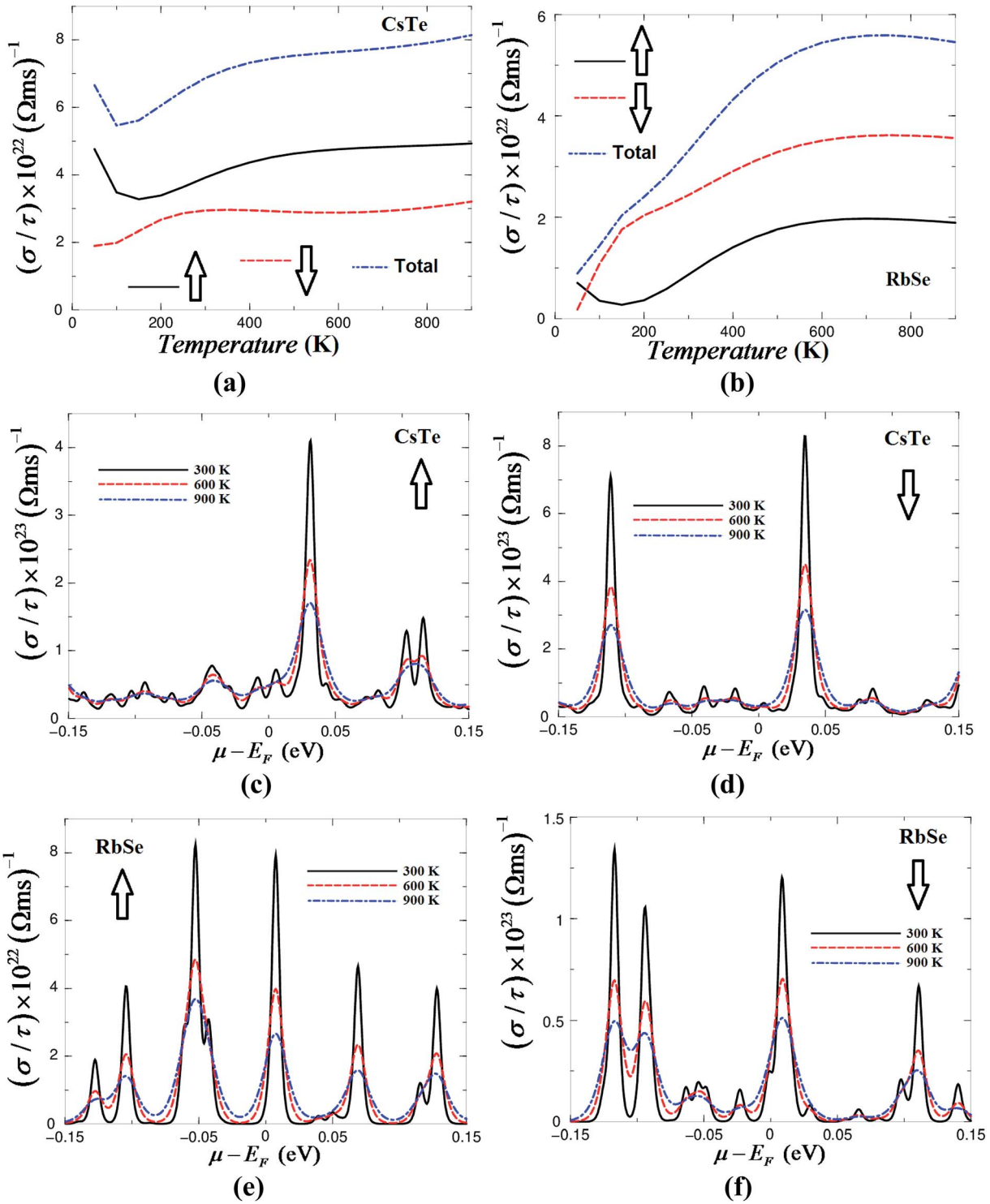

Fig. 5 (a and b) (σ/τ) for total and (↑)(↓) electrons *versus* temperature for CsTe and RbSe; (c and d) (σ/τ) for (↑)(↓) electrons *versus* chemical potential at three constant temperatures (300, 600 and 900) K for CsTe; (e and f) (σ/τ) for (↑)(↓) electrons *versus* chemical potential at three constant temperatures (300, 600 and 900) K for RbSe.

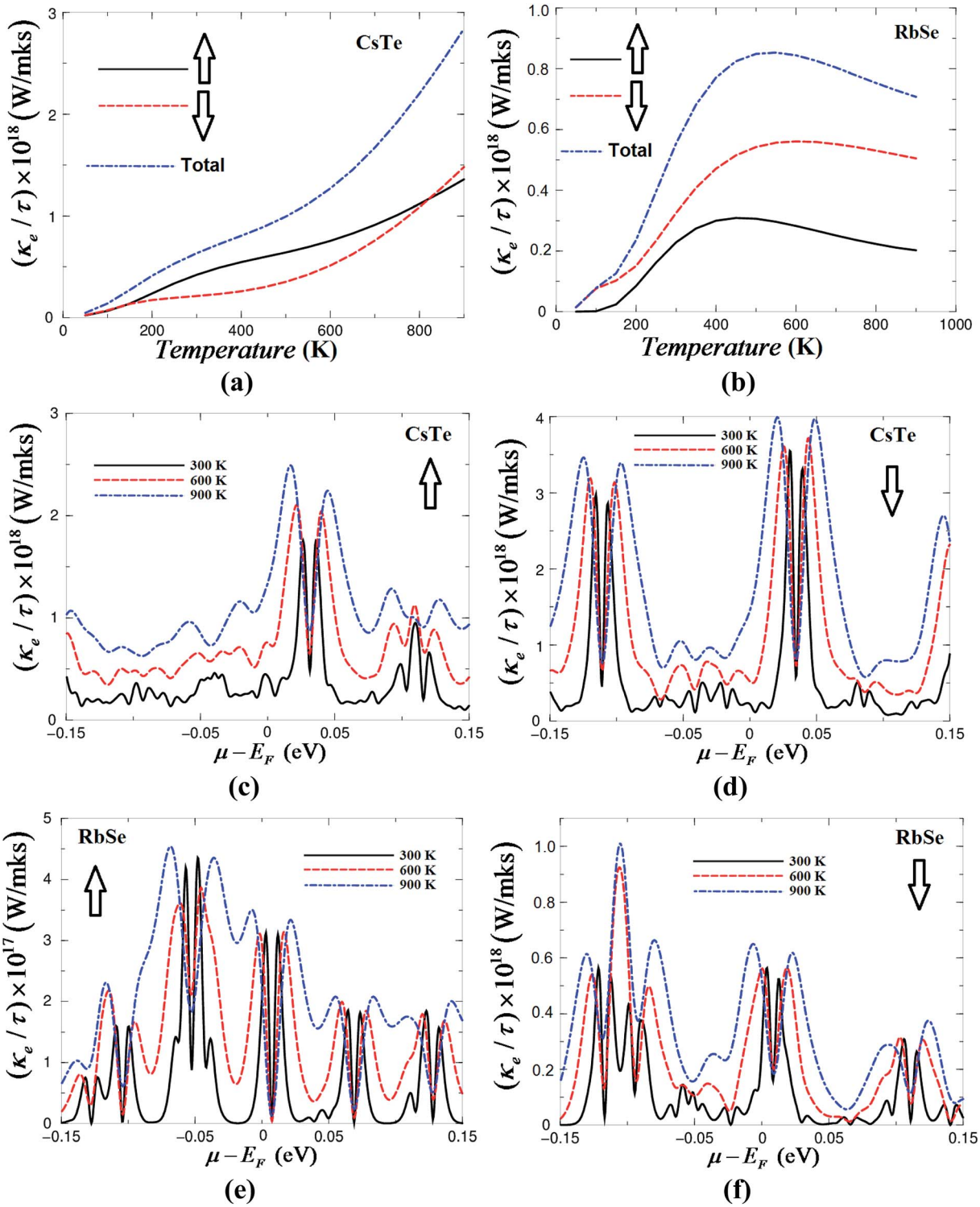

Fig. 6 (a and b) The electronic thermal conductivity for total and (↑)(↓) electrons *versus* temperature for CsTe and RbSe; (c and d) the electronic thermal conductivity for (↑)(↓) electrons *versus* chemical potential at three constant temperatures (300, 600 and 900) K for CsTe; (e and f) the electronic thermal conductivity for (↑)(↓) electrons *versus* chemical potential at three constant temperatures (300, 600 and 900) K for RbSe.

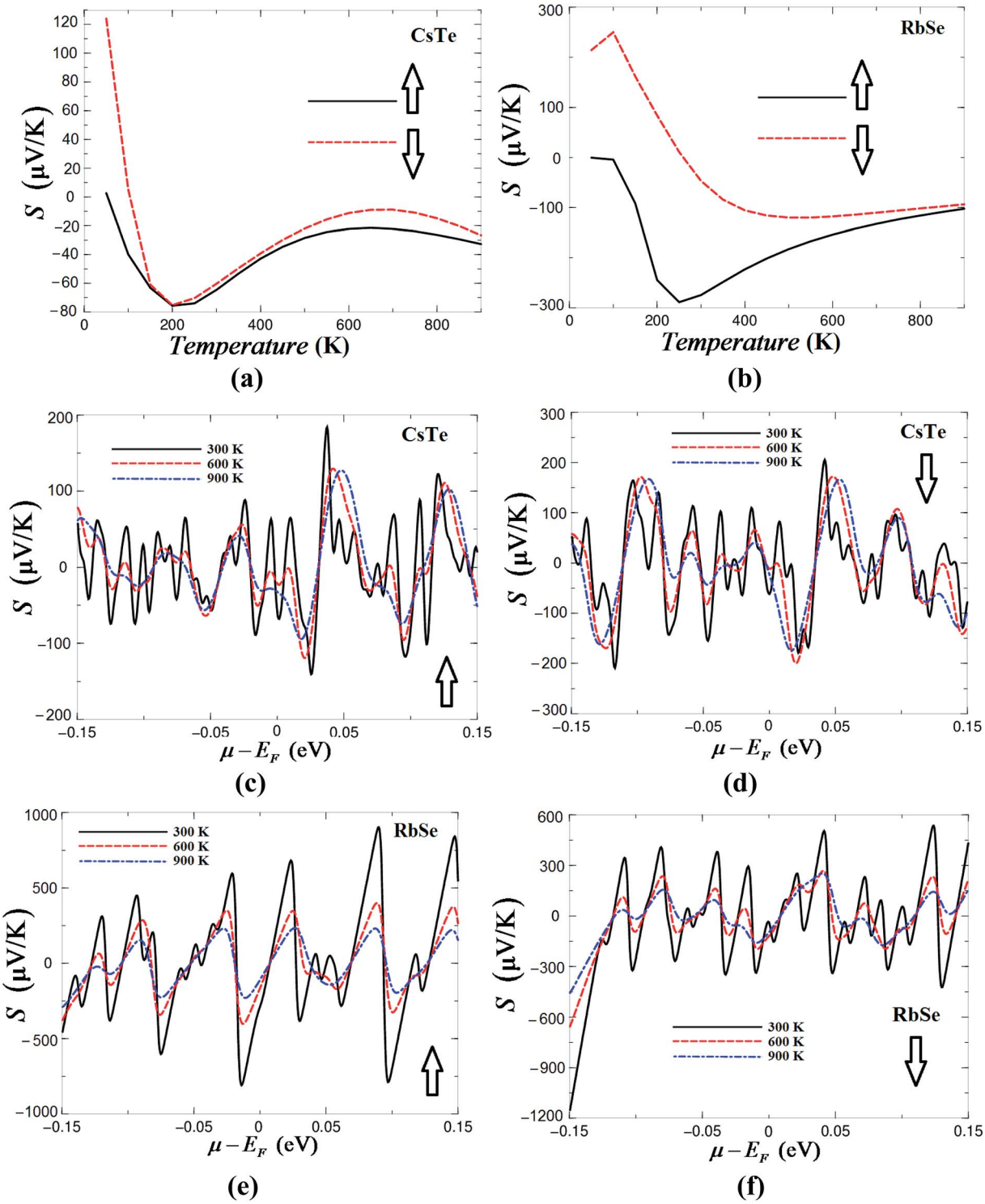

Fig. 7 (a and b) Seebeck coefficient (*S*) for (↑)(↓) electrons *versus* temperature for CsTe and RbSe; (c and d) *S* for (↑)(↓) electrons *versus* chemical potential at three constant temperatures (300, 600 and 900) K for CsTe; (e and f) *S* for (↑)(↓) electrons *versus* chemical potential at three constant temperatures (300, 600 and 900) K for RbSe.

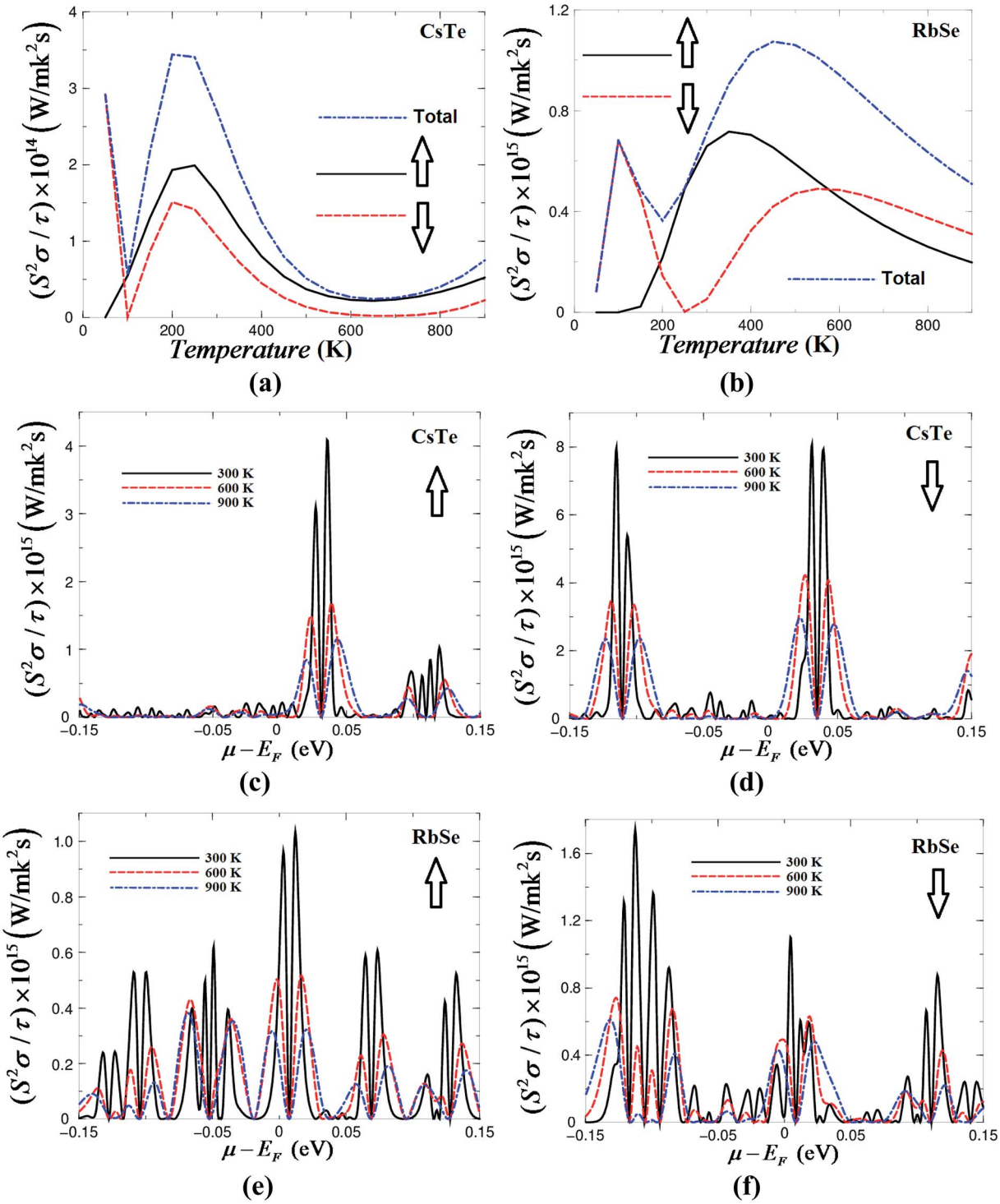

Fig. 8 (a and b) Power factor (*P*) for total and (↑)(↓) electrons *versus* temperature for CsTe and RbSe; (c and d) *P* for (↑)(↓) electrons *versus* chemical potential at three constant temperatures (300, 600 and 900) K for CsTe; (e and f) *P* for (↑)(↓) electrons *versus* chemical potential at three constant temperatures (300, 600 and 900) K for RbSe.

thermal conductivity.[24] The electrical conductivity $\sigma = ne(\eta_e + \eta_h)$ is proportional to n, η_e and η_h, where η_e and η_h are the electrons and holes mobility.† The mobility inversely depends on the effective mass ($\eta_e = e\tau_e/m_e^*$ and $\mu_h = e\tau_h/m_h^*$). Therefore, to gain high σ low effective mass and high n are required. The temperature dependent electrical conductivity (σ/τ) at a certain value of the chemical potential ($\mu = E_F$) for the spin-up/down channels of CsTe and RbSe are shown in Fig. 5a and b. It has been noticed that the trends of the spin-up/down and the total

† Here we use the symbol (η) for the mobility in order to distinguish it from the chemical potential (μ).

σ/τ for CsTe are differ than that of RbSe which is attributed to the carrier concentration, carrier's type and carrier's mobility. To ascertain this, we have investigated the $(\uparrow)(\downarrow)\sigma/\tau$ for both compounds at three constant temperatures as shown in Fig. 5c–f. It has been found that for all cases the 300 K induced the highest σ/τ at the vicinity of E_F, which is attributed to the fact that at temperature higher than 300 K the mobility increases dramatically resulting in an significant increase the carrier's scattering and hence reduces the electrical conductivity.

The temperature dependent $(\uparrow)(\downarrow)$ electronic thermal conductivity (k_e/τ) at a certain value of the chemical potential $(\mu = E_F)$ for CsTe and RbSe are shown in Fig. 6a and b. It has been noticed that the $(\uparrow)(\downarrow)k_e/\tau$ significantly increases with increasing the temperature and the trends of $(\uparrow)(\downarrow)k_e/\tau$ and the total k_e/τ for CsTe are differ than that of RbSe which is again attributed to the carrier concentration, carrier's type and carrier's mobility. It is clear that RbSe exhibit k_e/τ much lower than that of CsTe. Further, we have investigated the $(\uparrow)(\downarrow)k_e/\tau$ as a function of chemical potential at three different temperatures as shown in Fig. 6c–f. It confirm that $(\uparrow)(\downarrow)k_e/\tau$ show significant increase with increasing the temperature and RbSe exhibit k_e/τ much lower than that of CsTe.

The $(\uparrow)(\downarrow)$ Seebeck coefficient (S) as a function of temperature at a certain value of the chemical potential $(\mu = E_F)$ for CsTe and RbSe are illustrated in Fig. 7a and b. It show that at low temperature both compounds exhibit large S which decreases with increasing T and RbSe show larger S than that of CsTe. To ascertain this, we have plotted S as function of chemical potentials for three constant temperatures (Fig. 7c–f). It confirm that RbSe exhibit larger S than that of CsTe and the $(\downarrow)S$ of CsTe and RbSe are larger than that of $(\uparrow)S$ that is attributed to the fact that the valence electrons in CsTe are much more than that of RbSe. It has been reported that for an increase of the valence electrons the absolute value of S is decreased. This is explained by the increase of the electrons concentration in the bands. By increasing the number of valence electrons additional electrons are added to the d-band at the Fermi energy.[25] This leads to an increase of the n. The increase of the n leads to decrease S.[24] The interrelationship between n and S can be seen from relatively simple models of electron transport. For simple metals or degenerate semiconductors with parabolic bands and energy independent scattering S is given by;

$$S = \frac{8\pi^2 {k_B}^2}{3eh^2} m^* T \left(\frac{\pi}{3n}\right)^{3/2} \quad (1)$$

It can be clearly seen that S depends on n and m^*. The latter depend on the shape of the bands.

The power factor $(P = S^2\sigma/\tau)$ is an important quantity to evaluate the efficiency of the thermoelectric material since it is directly related to the dimensionless figure of merit $(ZT = S^2\sigma T/k_e + k_l)$.[9] As P is directly proportional to σ/τ and S^2 therefore, it is necessary to maintain the values of σ/τ and S^2. The $(\uparrow)(\downarrow)$ and total P as a function of T at a certain value of the chemical potential for CsTe and RbSe are shown in Fig. 8a and b. One can see that at a certain value of the chemical potential $(\mu = E_F)$ RbSe show higher P than that of CsTe. Whereas when we vary the chemical potential between $\mu - E_F = \pm 0.15$ (Fig. 8c–f) we noticed that CsTe show larger P than that of RbSe which is attributed to the fact that CsTe possesses much higher σ/τ than that of RbSe.

4. Conclusions

With the aid of the first-principles method (FPLAPW + lo) and the second-principles methods (BoltzTraP code) the thermoelectric properties of CsTe and RbSe are calculated for the ground state within the limits of Boltzmann theory. The recently modified Becke–Johnson potential (mBJ) is used to perform these calculations. The calculations show that CsTe and RbSe compounds exhibit half-metallic gap of about 0.06 (0.07) eV for CsTe (RbSe). The density of states at Fermi level (E_F), $N(E_F)$, and the bare electronic specific heat coefficient (γ) for the spin-down channels are obtained. It has been found that only the spin-down channel contributes to the states at E_F which should lead to unusual transport properties. Thus, the bands that cross E_F are responsible for the thermoelectric properties and the bands which are not crossing E_F will contribute negligibly small to the thermoelectric properties. It has been reported that the thermoelectric properties is related to the electrons in the system, and these electrons are defined through Fermi surface, which determine the electrical conductivity therefore, the Fermi surface of the spin-down channels are calculated. It has been found that CsTe exhibit power factor as a function of chemical potential larger than that obtained from RbSe which is attributed to the fact that CsTe possesses much higher electronic electrical conductivity than that of RbSe.

Acknowledgements

The result was developed within the CENTEM project, reg. no. CZ.1.05/2.1.00/03.0088, cofunded by the ERDF as part of the Ministry of Education, Youth and Sports OP RDI programme and, in the follow-up sustainability stage, supported through CENTEM PLUS (LO1402) by financial means from the Ministry of Education, Youth and Sports under the National Sustainability Programme I. Computational resources were provided by MetaCentrum (LM2010005) and CERIT-SC (CZ.1.05/3.2.00/08.0144) infrastructures.

References

1 H. Wang, W. Chu and H. Jin, *Comput. Mater. Sci.*, 2012, **60**, 224–230.
2 S. Walia, R. Weber, S. Balendhran, D. Yao, J. T. Abrahamson, S. Zhuiykov, M. Bhaskaran, S. Sriram, M. S. Strano and K. Kalantar-zadeh, *Chem. Commun.*, 2012, **48**, 7462–7464.
3 S. Walia, R. Weber, K. Latham, P. Petersen, J. T. Abrahamson, M. S. Strano and K. Kalantar-zadeh, *Adv. Funct. Mater.*, 2011, **21**, 2072–2079.
4 S. Walia, R. Weber, S. Sriram, M. Bhaskaran, K. Latham, S. Zhuiykov and K. Kalantarzadeh, *Science*, 2011, **4**, 3558–3564.

5 M. I. Katsnelson, V. Y. Irkhin, L. Chioncel and R. A. de Groot, *Rev. Mod. Phys.*, 2008, **80**, 315.
6 C. Felser, G. H. Fecher and B. Balke, *Angew. Chem., Int. Ed.*, 2007, **46**, 668.
7 B. Balke, S. Wurmehl, G. H. Fecher, C. Felser and J. Kübler, *Sci. Technol. Adv. Mater.*, 2008, **9**, 014102.
8 S. Sharma and S. K. Pandey, *J. Phys.: Condens. Matter*, 2014, **26**, 215501.
9 C. Calvin Hu, *Modern Semiconductor Devices for Integrated Circuits, Part I: Electrons and holes in a semiconductor*, 2011.
10 K. Uchida, S. Takahashi, K. Harii, J. Ieda, W. Koshibae, K. Ando, S. Maekawa and E. Saitoh, *Nature*, 2008, **455**, 778.
11 S. A. Wolf, D. D. Awschalom, R. A. Buhrman, J. M. Daughton, S. von Molnar, M. L. Roukes, A. Y. Chtchelkanova and D. M. Treger, *Science*, 2001, **294**, 1488.
12 I. Zutic, J. Fabian and S. D. Sarma, *Rev. Mod. Phys.*, 2004, **76**, 323.
13 C. Chappert, A. Fert and F. N. Van Dau, *Nat. Mater.*, 2007, **6**, 813.
14 H.-H. Xie, R.-Y. Ma, Q. Gao, L. Li and J.-B. Deng, *Chem. Phys. Lett.*, 2016, **661**, 89–93.
15 P. Blaha, K. Schwarz, G. K. H. Madsen, D. Kvasnicka and J. Luitz, *WIEN2k, An augmented plane wave plus local orbitals program for calculating crystal properties*, Vienna University of Technology, Austria, 2001.
16 J. P. Perdew, S. Burke and M. Ernzerhof, *Phys. Rev. Lett.*, 1996, **77**, 3865.
17 F. Tran and P. Blaha, *Phys. Rev. Lett.*, 2009, **102**, 226401.
18 G. K. H. Madsen and D. J. Singh, *Comput. Phys. Commun.*, 2006, **175**, 67–71.
19 P. B. Allen, in *Quantum Theory of Real Materials*, ed. J. R. Chelikowsky and S. G. Louie, Kluwer, Boston, 1996, pp. 219–250.
20 J. M. Ziman, *Electrons and Phonons*, Clarendon, Oxford, 2001.
21 C. M. Hurd, *The Hall Effect in Metals and Alloys*, Plenum, New York, 1972.
22 J. Kübler, A. R. Williams and C. B. Sommers, *Phys. Rev. B: Condens. Matter Mater. Phys.*, 1983, **28**, 1745.
23 S. Sharma and S. K. Pandey, *J. Phys.: Condens. Matter*, 2014, **26**, 215501.
24 G. J. Snyder and E. S. Toberer, *Nat. Mater.*, 2008, **7**, 105–114.
25 S. Ouardi, B. Balke, A. Gloskovskii, G. H. Fecher, C. Felser, G. Schönhense, T. Ishikawa, T. Uemura, M. Yamamoto, H. Sukegawa, W. Wang, K. Inomata, Y. Yamashita, H. Yoshikawa, S. Ueda and K. Kobayashi, *J. Phys. D: Appl. Phys.*, 2009, **42**, 084010.